minerals

MDPI

Article

Effect of H_2O_2 on the Separation of Mo-Bi-Containing Ore by Flotation

Shangyong Lin [1,2], Runqing Liu [1,2,*], Wei Sun [1,2], Yuehua Hu [1,2,*] and Haisheng Han [1,2]

1 School of Mineral Processing and Bioengineering, Central South University, Changsha 410083, China; linshangyong@csu.edu.cn (S.L.); sunmenghu@csu.edu.cn (W.S.); hanhai5086@csu.edu.cn (H.H.)
2 Key Laboratory of Hunan Province for Clean and Efficient Utilization of Strategic Calcium-Containing Mineral Resources, Central South University, Changsha 410083, China
* Correspondence: liurunqing@126.com (R.L.); hyh@csu.edu.cn (Y.H.); Tel.: +86-731-8883-6873 (R.L. & Y.H.)

Received: 31 July 2018; Accepted: 10 September 2018; Published: 13 September 2018

Abstract: Hydrogen peroxide (H_2O_2) is a strong oxidizer that causes non-selective oxidation of sulfide minerals, and its influence on bismuth sulfide ores is not well-documented. In this study, H_2O_2 was proposed as an alternative bismuthinite depressant, and its effect on a Mo-Bi-containing ore was intensively investigated by batch flotation tests. Results showed that the addition of H_2O_2 significantly destabilized the froth phase, thus decreasing the solids and water recovery. The recovery of bismuth in molybdenum concentrate was dramatically decreased to 4.64% by H_2O_2 compared with that in the absence of H_2O_2 (i.e., 50.14%). The modified first-order kinetic model demonstrated that the flotation rate of molybdenite slightly declined after H_2O_2 addition, whereas that of bismuthinite was drastically reduced from 0.30 min^{-1} to 0.08 min^{-1} under the same condition. Simulation revealed that H_2O_2 affected the floatability of both molybdenite and bismuthinite but resulted in more detrimental effect to bismuthinite. Hence, H_2O_2 has the potential to act as an effective depressant in bismuth sulfide ore flotation.

Keywords: molybdenite; bismuthinite; hydrogen peroxide; froth flotation

1. Introduction

The Shizhuyuan mine is one of the largest polymetallic deposits in the world, having been famous for its W-Sn-Mo-Bi mineralization zone since exploited in the 1960s [1,2]. The Shizhuyuan orefield is located in Hunan province, China, which is 15 km from the southeast of Chenzhou city [3,4], and includes 750,000 t WO_3, 490,000 t Sn, 300,000 t Bi, 130,000 t Mo, and 76,000,000 t fluorite [4]. In Dongpo dressing plant, Shizhuyuan ore is first treated with bulk sulfide flotation, followed by tungsten mineral flotation, and fluorite is recovered in the last section. Figure 1 shows the flotation flowsheet of Dongpo dressing plant.

During sulfide flotation, most of the sulfide minerals float, forming Mo-Bi-Fe rougher concentrate. Then, the differential flotation separation of Mo-Bi-Fe sulfide minerals is carried out to produce three distinct Mo, Bi, and Fe concentrates. However, the efficient separation of molybdenite from bismuthinite is a challenge for mineral-processing industries due to their similar flotation behavior. As an environmentally friendly valuable metal, bismuth is widely used in cosmetics and pharmaceuticals [5]. A high flotation recovery of bismuth is undesirable for the final molybdenum flotation concentrates because smelters would not pay for excessive bismuth levels on molybdenum concentrates. Besides, it is uneconomic and inefficient to remove or recover Bi from the Mo concentrate during hydrometallurgy. The efficient and inexpensive separation of bismuthinite from molybdenite at the early stage, such as flotation, is especially important.

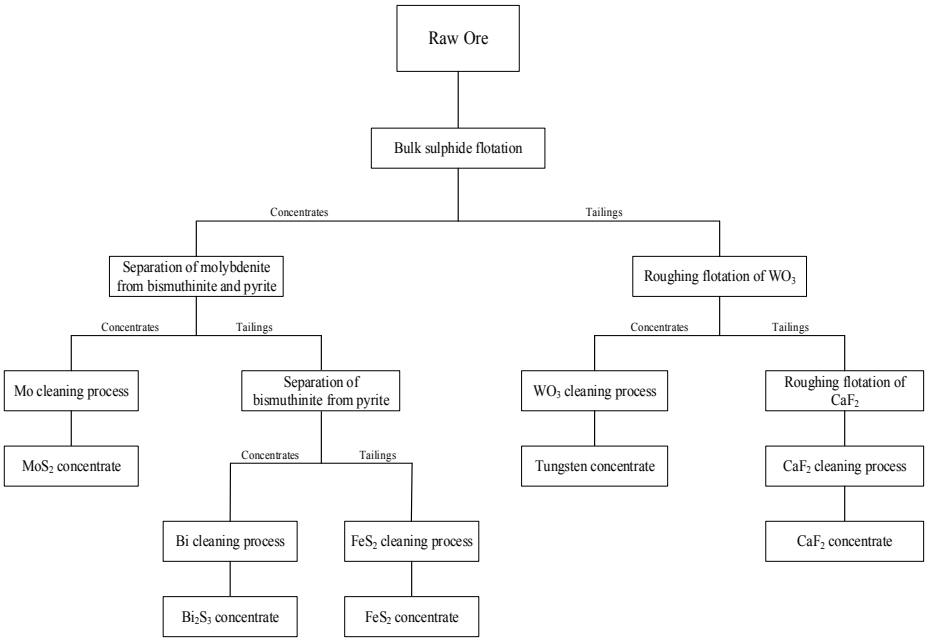

Figure 1. The flotation flowsheet of the Shizhuyuan ore in Dongpo dressing plant.

In the mineral-processing industry, a series of inorganic depressants such as sodium sulfide (Na_2S), sodium hydrosulfide (NaHS), potassium dichromate ($K_2Cr_2O_7$), or their combination, are routinely used to depress the bismuth sulfide minerals [6–8]. A predominant disadvantage of these inorganic depressants is that most of them are toxic and harmful. Their use is under increasing pressure due to increasingly rigid environmental pollution control regulations [9]. These inorganic depressants cannot lower the mechanical entrainment of the depressed minerals and require large dosages in the mineral industry [10,11]. As an alternative, polysaccharides have been developed and utilized in sulfide mineral separations. Dextrin is a very effective molybdenite flotation depressant in the absence of a collector [12]. Carboxymethyl cellulose was used to depress bismuthinite and galena during Mo-Bi-Pb separation [13]. However, the use of polysaccharides in froth flotation is associated with non-specific inhibition of all sulfide minerals [14–16], which hinders its wider application in mineral-processing plants.

Another important method utilizing oxidants such as hydrogen peroxide (H_2O_2) have been reported. H_2O_2 is a strong oxidizer that can produce hydroxyl (OH·) and hydroperoxyl radicals (OOH·), which are a much more effective oxidant [17,18]. In most cases, H_2O_2 presents a disadvantageous effect on sulfide mineral flotation due to the formation of hydrophilic oxidation products (e.g., $Pb(OH)_2$, $Cu(OH)_2$, FeOH, and FeOOH) that precipitate on the mineral surface [19–21]. Hypothetically, H_2O_2 could give a similar result on the separation of molybdenite and bismuthinite. Nevertheless, no readily available literature reports the influence of H_2O_2 on bismuthinite. The detailed depression mechanism of H_2O_2 during flotation of natural sulfide ore has not been explained. Hence, the objective of the present work was to investigate the holistic influence of H_2O_2 on the flotation performance of a Mo-Bi-containing ore from Shizhuyuan.

Solids and water recovered to the concentrate are also monitored to evaluate the influence H_2O_2 on the froth behavior. The ore in the concentrate is composed of minerals recovered by flotation and minerals recovered by entrainment [22,23]. The amount of entrained minerals is related to that of water recovered to the concentrate [24,25]. The quantity of water recovered to the concentrate is directly dependent on the stability of the froth phase [26]. In general, high water and solids recovery indicate a greater froth stability, whereas a lower value indicates a less stable froth [17]. Solids and water recovery is not directly affected by flotation reagents, but is affected by the changes in froth stability brought by reagent addition [27]. In practice, the recovery of solid and water to the concentrate is usually used to represent the effect of flotation agents on the properties of froth behavior [17,28].

The froth behavior in the absence and presence of H_2O_2 was studied to understand the effect of H_2O_2 on the froth phase. The depression mechanism of H_2O_2 on bismuthinite and molybdenite was discussed by modifying the first-order flotation rate constant analysis and Pourbaix diagram analysis.

2. Materials and Methods

2.1. Samples and Reagents

2.1.1. Samples

The typical ore (Mo-Bi-containing sulfide ore), supplied by Dongpo (the ore field of Shizhuyuan), was crushed through a jaw crusher to obtain a particle size of 100% passing 3 mm. The X-ray diffraction (XRD) analysis indicated that the major sulfide minerals were molybdenite, bismuthinite, and pyrite. The main gangue minerals were fluorite, quartz, garnet, and calcite. The results are shown in Table 1. The synthetic bismuthinite was purchased from HAOXI Research Nanomaterials, Inc., Shanghai, China. The synthetic bismuthinite sample was 99.99% in purity. Molybdenite was obtained from China Molybdenum Co., Ltd (Luoyang, China). The molybdenite sample was 92.14% in purity.

Table 1. Minerals (sulfide and gangue) present in the ore as determined using XRD.

Mineral	Wt %	Mineral	Wt %
Bismuthinite	0.10	Sericite	4.50
Molybdenite	0.08	Chlorite	3.50
Scheelite	0.37	Hornblende	2.00
Wolframite	0.05	Kaolinite	2.00
Cassiterite	0.09	Feldspar	2.00
Bismutite	0.02	Diopside	1.50
Magnetite	2.00	Idocrase	0.50
Pyrite	1.20	Calcite	7.00
Fluorite	21.50	Dolomite	1.00
Quartz	20.00	Other	0.59
Garnet	30.00	Total	100.00

2.1.2. Reagents

Industry-grade kerosene and terpilenol were used as collector and frother, respectively, and were used as received. The pH of the pulp during flotation was adjusted by the addition of NaOH and HCl. Analytical grade H_2O_2 was supplied at 30% purity with no further dilution. Tap water was used in all flotation experiments. All chemical solutions were freshly prepared daily.

2.2. Batch Flotation Experiments

One kilogram of crushed ore was ground in a stainless-steel ball mill combined with 500 mL tap water, to achieve a P80 of 75 μm. After grinding, the pulp was transferred to a 3 L XFD-63 single-stage flotation cell. The pulp density in the flotation cell was made up to 30% solids by the addition of tap water. The nature pH of the slurry was ~8 and was fixed at 8 by using NaOH or HCl before addition. H_2O_2, collector, and frother were added into the cell in sequence, and 3 min of conditioning time was required for each reagent. The agitation speed of 1950 rpm was maintained, and an airflow rate was set to 3 m^3/h. During flotation, the pulp level was controlled manually throughout by adding tap water. The froth was scraped every 15 s for 20 min. Four concentrates were collected into a pre-weighted collection tray after 2, 6, 12, and 20 min of flotation. The froth was maintained at the height of 2 cm throughout each test by constantly adding tap water. The solids and water recovered to the concentrate were monitored throughout to indicate the froth stability [29,30]. The amount of water recovered is calculated by subtracting the mass of solids and wash water from the mass of the total concentrate material. Concentrates and tails were filtered, dried, and weighed before being assayed for

molybdenum and bismuth by using an AxiosmAX X-ray Fluorescence (Malvern Panalytical, Shanghai, China). All experiments were conducted in duplicate.

The pulp potential (Eh) (vs. Standard Hydrogen Electrode, SHE) and pH were measured using PHS-3E pH meter (Shanghai INESA Scientific Instrument Co., Ltd., Shanghai, China). The calibration of pH meter was carried out daily, according to the manual, before experiments.

2.3. Thermodynamic Calculations

HSC Chemistry 6.0 was applied to calculate the Pourbaix diagrams for Mo-S-H_2O and Bi-S-H_2O systems to discuss the thermodynamic feasibility and flotation behavior of both MoS_2 and Bi_2S_3. The thermodynamic data used in this work are listed in Tables 3 and 4. Most of the data are adopted from the HSC 6.0 software database, which is a commonly used thermochemical software package.

2.4. Flotation Kinetics Model

The kinetics of flotation has been widely studied and is often used to analyze the effect of various parameters for flotation process [31–33]. Various flotation rate models are available, such as the first-order reaction [34], second-order kinetics [35], and thirteen-rate models [32]. Among these models, the modified first-order kinetic model proposed by Agar [36] is a well-known classical kinetic model. Xu [31] introduced the concept of a selectivity index into the classical kinetic model to simplify the data comparison. The modified first-order kinetic model can be mathematically expressed as follows:

$$R = R_{max}\left(1 - e^{-kt}\right) \tag{1}$$

$$K_M = R_\infty \cdot k = \left.\frac{\partial R}{\partial t}\right|_{t=0} \tag{2}$$

$$S.I._{(\mathrm{I/II})} = \frac{K_M \text{ of Mineral I}}{K_M \text{ of Mineral II}} \tag{3}$$

where R is the cumulative recovery at time t, R_{max} is the maximum theoretical flotation recovery, k is the first-order rate constant (min^{-1}), t is the cumulative flotation time (min), K_M is the modified flotation rate constant, and $S.I._{(\mathrm{I/II})}$ is the selectivity index of mineral I over mineral II. All tests in this study were performed by using the same particle size and operating conditions during flotation. The modified kinetic model can be used to investigate whether the H_2O_2 addition would affect the kinetics of flotation.

2.5. X-ray Photoelectron Spectroscopy

Freshly ground molybdenite and freshly prepared synthetic bismuthinite were used for X-ray photoelectron spectroscopy (XPS) samples. The experimental procedure was performed as previously described [11,19]. The XPS results of the treated and untreated samples were obtained with a K-Alpha 1063 spectrometer (Thermo Scientific Co., Waltham, MA, USA) at ambient temperature. The experiment was conducted using an Al Kα sputtering-ray source operated at 12 kV and 6 mA. The pressure in the analytical chamber at the time of analysis was 1.0×10^{-12} Pa. All binding energy calibration was based on the neutral C 1*s* peak at 284.8 eV to compensate for the surface charging effects. Data from the XPS tests were analyzed with XPS Peak 4.1 software.

3. Results and Discussion

3.1. Flotation Performances

Figure 2 shows the total solids and water recovered to the concentrate as a function of H_2O_2 concentration. The absence of H_2O_2 has the highest water and solids recovery. The mass of solids and water significantly decrease with increasing H_2O_2 concentration. Figure 3 depicts the average

cumulative mass of solids versus water at different H_2O_2 concentrations. The response to the different H_2O_2 concentration has the same trend. The highest amount of solids per unit water was obtained in the absence of H_2O_2. Increasing the H_2O_2 concentration from 0% to 0.02% causes a significant reduction in both solids and water recovered. The amount of solids per unit water for the concentration of 0.02%–0.04% was relatively similar, accompanied with a slight increase. Clearly, the solids and water recovery substantially decreases with increasing H_2O_2 dosage, which suggests that H_2O_2 has a significant effect on the froth stability.

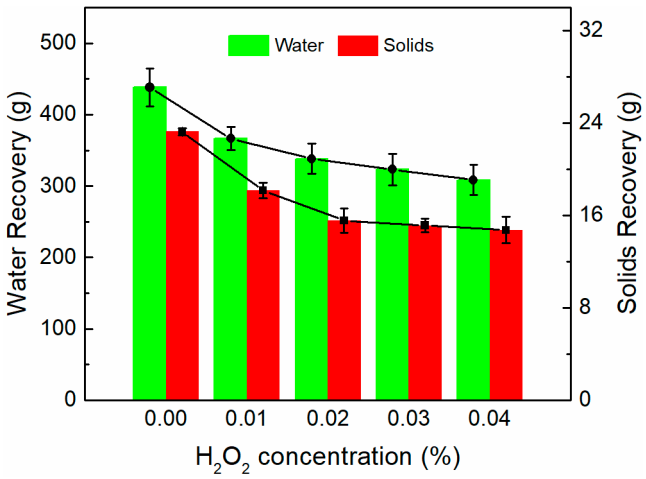

Figure 2. Total solids and water recovery from the concentrate as a function of H_2O_2 concentration. Error bars represent the standard deviation between duplicate tests.

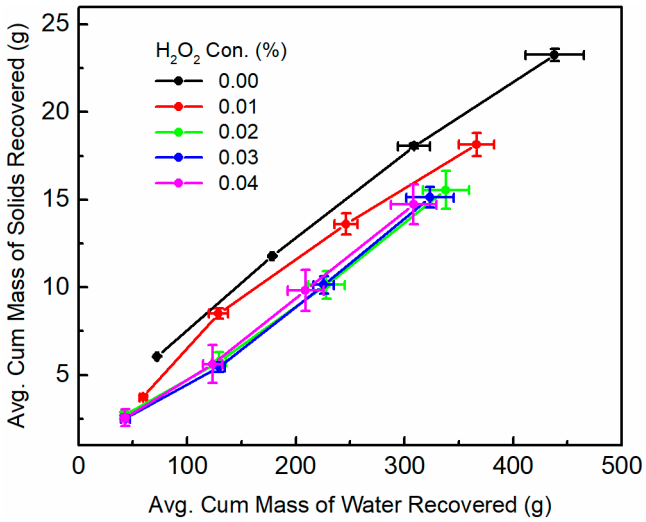

Figure 3. Average cumulative mass of solids versus water at different H_2O_2 concentrations. Error bars represent the standard deviation between duplicate tests.

The Eh and pH have a strong effect on the froth phase during flotation [37] which can be altered by H_2O_2. To eliminate the effect of pH and Eh on the froth stability, its variation was recorded after adding H_2O_2. Figure 4 shows the changes on Eh and pH after adding H_2O_2 to the pulp. In the presence of H_2O_2, the nature Eh was about −57 mv, and the nature pH was around 8. As the H_2O_2 concentration increased from 0% to 0.04%, the Eh slightly increased to −49 mv, which had no significant effect on the pH. The variation of Eh was very small and that of pH was negligible.

It is unlikely for Eh to directly affect the solids recovery because the solids recovered to the concentrate cannot be ascribed to the recovery of molybdenite and bismuthinite alone. The content of molybdenite and bismuthinite in the Shizhuyuan ore is only in the region of 0.08% and 0.10%,

respectively, which is equivalent to 1.8 g for 1 kg of ore used in each batch flotation. The mass of the solids recovered to the concentrate is in the range of 14–24 g. The solids recovered are dominated by gangue minerals, rather than sulfide minerals. All batch flotation tests were done under the same particle size distribution and solids density [38]; hence, the decrease in the solids and water recovery can be attributed to the addition of H_2O_2. The significant decrease in water and solids recovery may also be an indication that H_2O_2 has an impact on the froth phase during flotation.

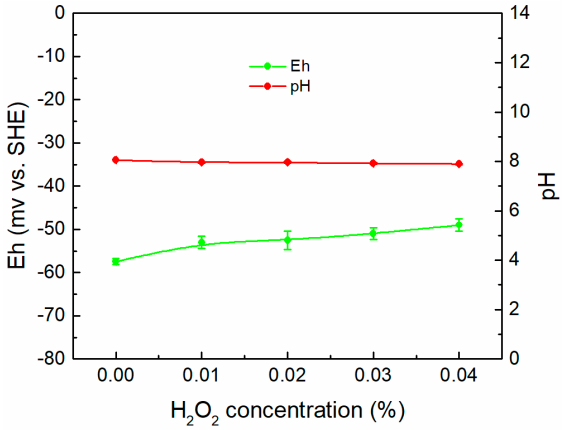

Figure 4. Variations on Eh and pH as a function of H_2O_2 concentration. Error bars represent the standard deviation between duplicate tests.

Figure 5 shows the recovery and grade of molybdenum and bismuth at pH 8. In the absence of H_2O_2, the recovery of molybdenum and bismuth were 80% and 50.14% with a grade of 2.0% and 1.71%, respectively. After adding H_2O_2, the final recovery of molybdenum was slightly decreased, accompanied with an increase in grade (Figure 5A). Combined with the analysis of Figures 2 and 3, the increase in Mo grade is easily ascribed to the lower recovery of solids from the concentrate because most solids in the concentrate are gangue minerals. As for bismuthinite, the final recovery and grade of bismuth was sharply decreased under the same conditions (Figure 5B). When the concentration of H_2O_2 increased to 0.02%, the final recovery and grade of bismuth drastically decreased to 4.64% and 0.22%, respectively. The results indicate that H_2O_2 exhibits an inhibition to bismuthinite and a negligible effect to molybdenite.

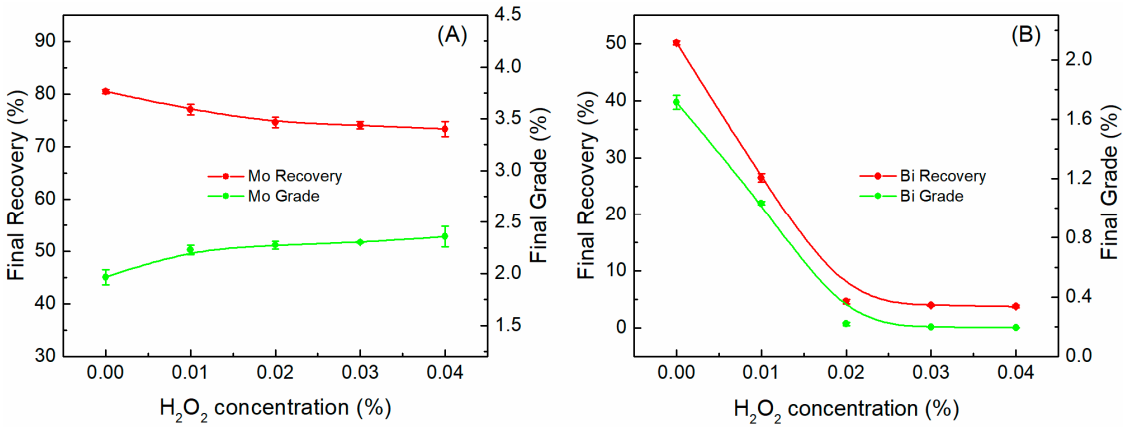

Figure 5. Final recovery and grade as a function of H_2O_2 concentration: (**A**) molybdenum, (**B**) bismuth. Error bars represent the standard deviation between duplicate tests.

The depressing effect of H_2O_2 could also be observed from the viewpoints of selectivity between molybdenite and bismuthinite. Figure 6 illustrates the curves of Mo recovery versus Bi recovery with different H_2O_2 concentrations. The results demonstrated that H_2O_2 could selectively depress

bismuthinite and maintain a higher recovery for molybdenite. The flotation with the addition of H_2O_2 floated less bismuth minerals than that without adding H_2O_2. Thus, the H_2O_2 improved the selectivity between molybdenite and bismuthinite in flotation.

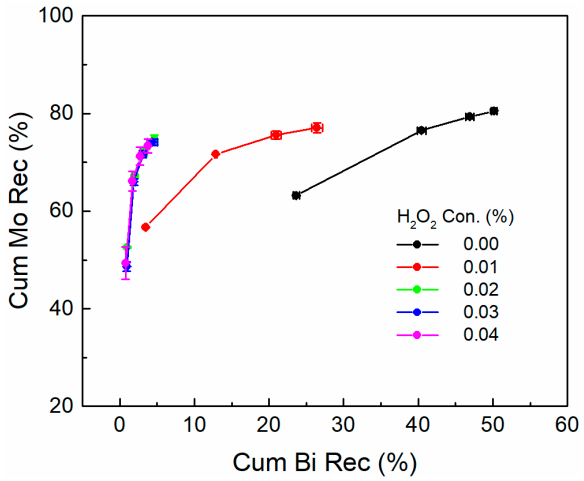

Figure 6. Effect of H_2O_2 addition on Mo concentrate and its selectivity against bismuthinite. Error bars represent the standard deviation between duplicate tests.

3.2. Flotation Kinetics

The maximum theoretical flotation recoveries of molybdenum and bismuth and the first-order rate constant obtained from the fitting curves at each H_2O_2 concentration are presented in Table 2. The molybdenum/bismuth sulfide selectivity index ($S.I._{(Mo/Bi)}$) deduced from the model parameters data was also tabulated in Table 2. Figure 7 shows the recovery of molybdenum and bismuth as a function of flotation time, and the solid lines stand for the model fit.

As shown in Figure 7A, the recovery of molybdenum was comparatively high. The addition of H_2O_2 resulted in a slightly lower Mo recovery than the case without H_2O_2. However, the molybdenum recovery did not vary much with H_2O_2 concentration. From Table 2, as H_2O_2 concentration increased from 0% to 0.04%, the ultimate recovery of molybdenum decreased from 80.51% to 73.36%, following the decrease in rate constant from 0.76 min^{-1} to 0.46 min^{-1}. With respect to bismuthinite (Figure 7B), both R_{max} and k sharply decreased with the increase in H_2O_2 concentration. The ultimate recovery of bismuth drastically decreased from 50.14% to 4.50%, corresponding to the decrease in rate constant from 0.30 min^{-1} to 0.08 min^{-1}. The data indicate that H_2O_2 exerts a negligible influence on the depression of molybdenite but has an obvious depression effect on bismuthinite.

The calculated selectivity index (*S.I.*) presented in Table 2 is 4.07 in the absence of H_2O_2, and the $S.I._{(Mo/Bi)}$ value was considerably increased to 99.48 when the H_2O_2 concentration was increased to 0.02%. The high *S.I.* values of molybdenite over bismuthinite obtained in the presence of H_2O_2 indicate that H_2O_2 has a higher separation selectivity for molybdenite and bismuthinite. The addition of H_2O_2 increased the selectivity of molybdenite against bismuthinite and to a large extent than that observed initially.

Table 2. Model parameters of flotation kinetics obtained under different H_2O_2 concentrations at pH 8.

H_2O_2 Concentration (%)	MoS_2		Bi_2S_3		$S.I._{(Mo/Bi)}$
	k (min^{-1})	R_{max} (%)	k (min^{-1})	R_{max} (%)	
0.00	0.76	80.51	0.30	50.14	4.07
0.01	0.63	77.07	0.10	30.50	15.92
0.02	0.60	74.61	0.09	5.00	99.48
0.03	0.46	74.13	0.09	5.00	75.78
0.04	0.46	73.36	0.08	4.50	93.74

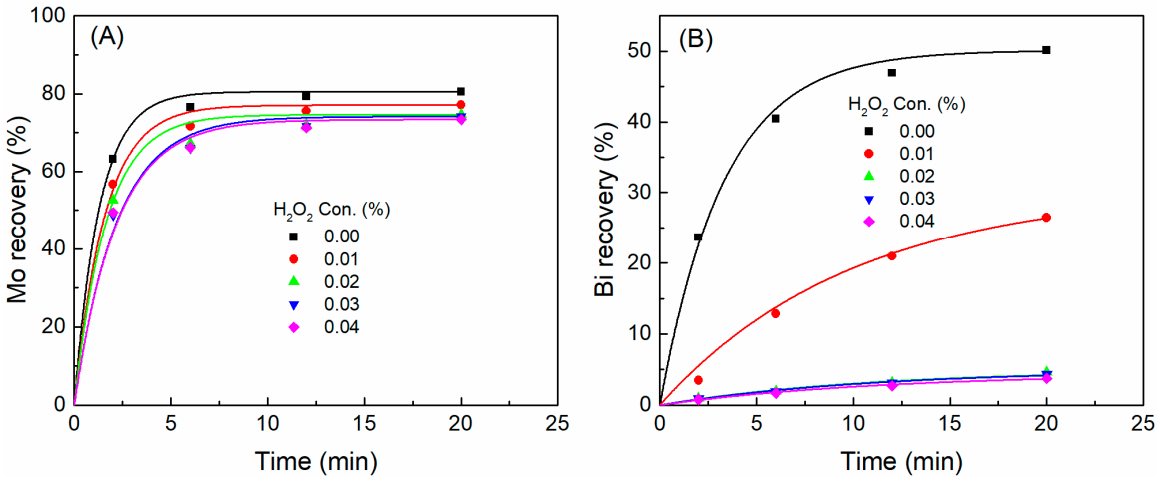

Figure 7. Flotation rate under various H_2O_2 concentrations: (**A**) molybdenite, (**B**) bismuthinite. Solid line represents the best fit curve.

The cumulative grade-recovery curves for molybdenum and bismuth are shown in Figure 8, respectively. As shown in Figure 8A, a molybdenum recovery of 63% was achieved after 2 min of flotation of the Shizhuyuan ore in the absence of H_2O_2. After adding H_2O_2, a marginal decline in the recovery of molybdenum occurred, but a considerable rise in grade for the concentrate collected was observed at the first two minutes. However, the final recovery of molybdenum gradually decreased from 80% to 74% in the H_2O_2 concentration range of 0%–0.04%, and the grade of molybdenum was almost identical under the same H_2O_2 concentration range. This is an interesting phenomenon, because the *k* value derived from Equation (1) presents a downward trend when H_2O_2 is taken into the pulp (Table 2). As mentioned above, the presence of H_2O_2 results in lower solids and water recoveries from the concentrate (Figures 2 and 3). Therefore, it can easily be deduced that the increase of molybdenum grade at the early stage (first concentrate) is ascribed to the lower recovery of solids.

In the case of bismuthinite (Figure 8B), the increase in H_2O_2 concentration shifts the grade-recovery curve to the lower left corner. Both the recovery and grade of bismuth decreased throughout the flotation process after adding H_2O_2. The final recovery of bismuth dropped from 50% to 4% as the H_2O_2 concentration is increased from 0% to 0.04%. The observations demonstrate that the recovery difference between molybdenite and bismuthinite is continuously enlarged as the H_2O_2 concentration increases.

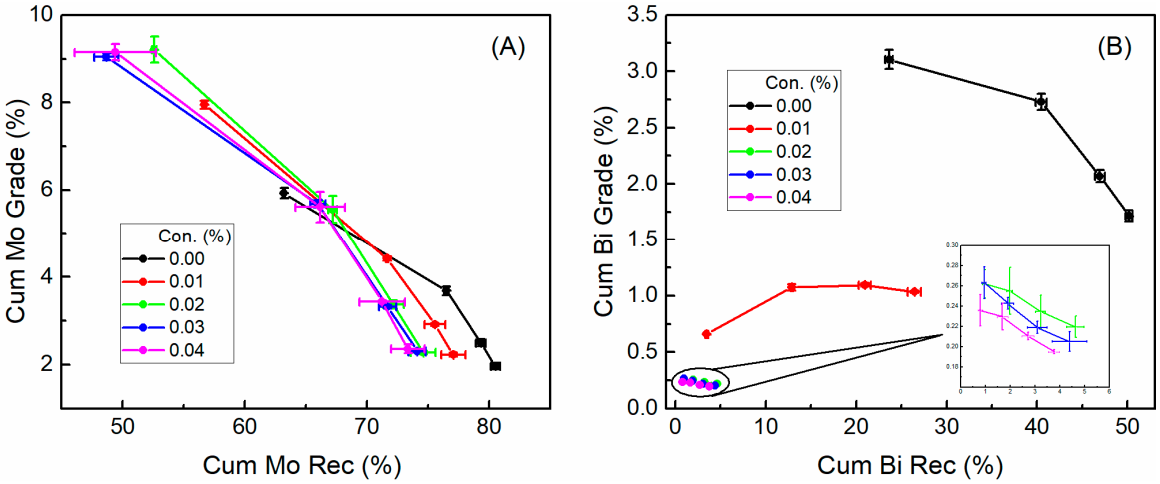

Figure 8. Cumulative grade versus recovery curves for different H_2O_2 concentrations: (**A**) molybdenite, (**B**) bismuthinite. Error bars represent the standard deviation between duplicate tests.

3.3. Eh–pH Diagram

The Eh–pH diagrams for the Mo-S-H_2O, S-Mo-H_2O, Bi-S-H_2O, and S-Bi-H_2O systems are shown in Figures 9–12. The upper grey dot lines drawn in each diagram represent O_2/H_2O, and the lower grey dot lines represent the H_2O/H_2 stability boundaries. The corresponding Gibbs free energy of formation ($\Delta_f G_m^\theta$/kJ·mol^{-1}) for species at 298.15 K are listed in Tables 3 and 4, respectively.

Bismuthinite crystals are orthorhombic, commonly massive with foliated or fibrous texture [39], with crystals of up to 12 cm, stout prismatic to acicular, elongated and striated [40]. Bismuth from the bismuthinite surface can exist as solid species and oxide precipitate (e.g., BiO) on the surface in a potential range of −100 mv to 100 mv at pH 8 (Figure 11). The molybdenum from the molybdenite surface can exist as stable ions MoO_4^{2-} (Figure 9), and the sulfur from molybdenite and bismuthinite surface can exist as SO_4^{2-} ions under the same conditions (Figures 10 and 12). During flotation, the potential of the pulp varied from −57 mv to −49 mv (vs. SHE) with the H_2O_2 concentration increased from 0% to 0.04%. It is expected that oxides will be formed on the bismuthinite surface in this potential region. Therefore, the decrease in the floatability of bismuthinite is likely due to the precipitation of oxidation products (e.g., BiO) on its surface, which renders the mineral hydrophilic.

The hydrophilic oxidation products on the molybdenite surface can dissolve as MoO_4^{2-} and SO_4^{2-} ions; hence, the surface of molybdenite should remain hydrophobic. However, the flotation results show that the recovery of molybdenite slightly decreases with the addition of H_2O_2 in aqueous solution. This phenomenon may be attributed to the degree of surface oxidation and the dissolution rate of oxidation products, according to the analysis of Hirajima et al. (2017) [19]. At a low concentration of H_2O_2, the surface of molybdenite was slightly oxidized by H_2O_2, resulting in a low concentration of oxidation products. The low concentration of oxidation products on the molybdenite surface resulted in a low dissolution rate from the molybdenite surface to the bulk solution. The formation rate of oxidation products on the surface of molybdenite was faster than the dissolution rate of oxidation products from its surface. Thus, the molybdenite surface is still covered by oxidation products, which reduces its floatability.

Table 3. The standard Gibbs free energy of formation for species considered in Figures 9 and 10.

Compound	**Mo**	**MoS_2**	**MoO_2**	**$MoO_3{\cdot}H_2O$**	**$HMoO_4^-$(a)**	**MoO_4^{2-}**
$\Delta_f G_m^\theta$/kJ·mol^{-1}	0.00	−63.86	−127.17	−219.15	−207.61	−199.85
Compound	**HS^-(a)**	**$S_4O_3^{2-}$(a)**	**$S_3O_3^{2-}$(a)**	**SO_4^{2-}(a)**	**HS_2O^{7-}(a)**	**HS_2O^{8-}(a)**
$\Delta_f G_m^\theta$/kJ·mol^{-1}	2.97	−228.82	−197.70	−177.91	−328.06	−360.97

(a): aqueous ions.

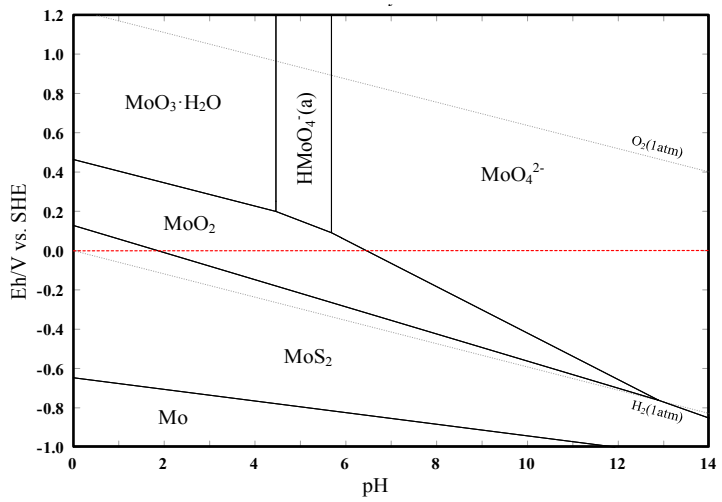

Figure 9. The Eh–pH diagram for the Mo-S-H_2O system. Conditions: 1×10^{-4} M molybdenum, 2×10^{-4} M sulfur, 298.15 K, 1 atm.

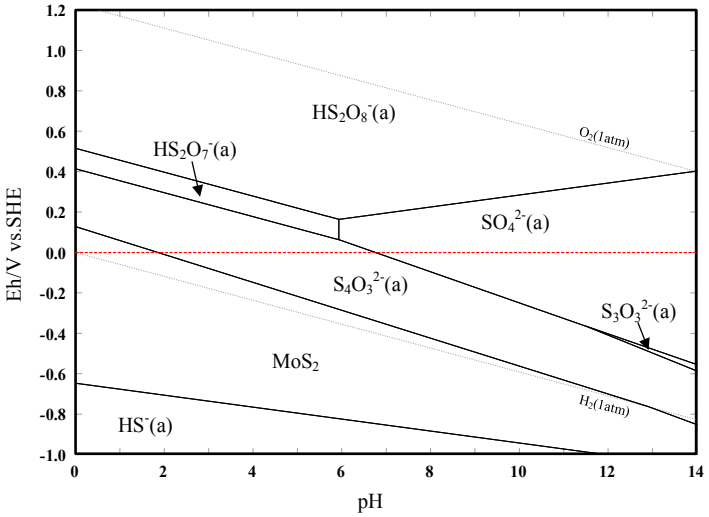

Figure 10. The Eh–pH diagram for the S-Mo-H_2O system. Conditions: 2×10^{-4} M sulfur, 1×10^{-4} M molybdenum, 298.15 K, 1 atm.

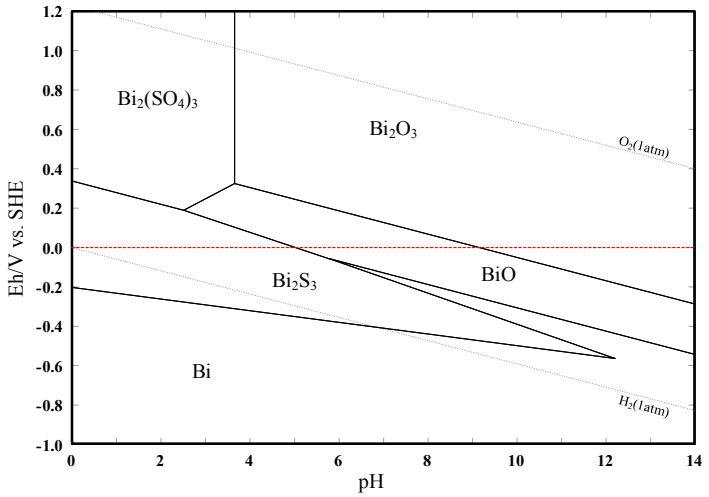

Figure 11. The Eh–pH diagram for the Bi-S-H_2O system. Conditions: 2×10^{-4} M bismuth, 3×10^{-4} M sulfur, 298.15 K, 1 atm.

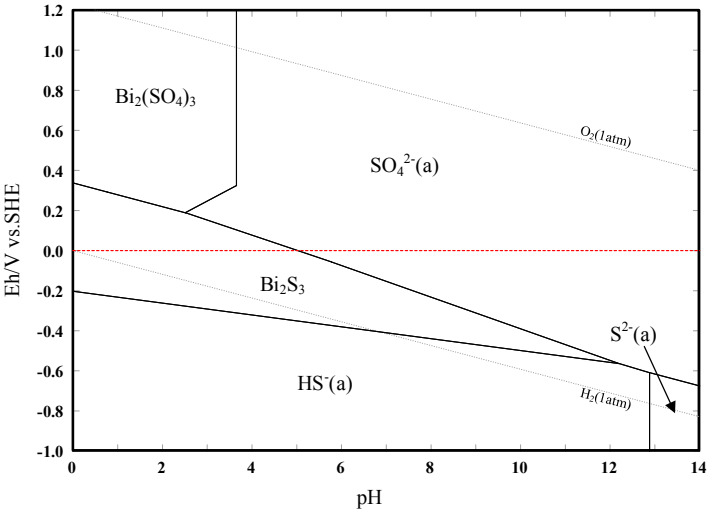

Figure 12. The Eh–pH diagram for the S-Bi-H_2O system. Conditions: 3×10^{-4} M sulfur, 2×10^{-4} M bismuth, 298.15 K, 1 atm.

Table 4. The standard Gibbs free energy of formation for species considered in Figures 11 and 12.

Compound	Bi	Bi_2S_3	BiO	$Bi_2(SO_4)_3$
$\Delta_f G_m^\theta$/kJ·mol^{-1}	0.00	−33.54	−43.54	−526.83
Compound	**Bi_2O_3**	**HS^- (a)**	**S^{2-} (a)**	**SO_4^{2-} (a)**
$\Delta_f G_m^\theta$/kJ·mol^{-1}	−118.81	2.97	19.06	−177.91

(a): aqueous ions.

3.4. XPS Analysis

XPS was conducted to analyze the surface chemistry of molybdenite and bismuthinite with and without H_2O_2 treatment. Figure 13A–C shows the XPS spectra of Mo 3*d*, S 2*p*, and O 1*s*, respectively. The Mo 3*d* spectra are best fitted with three peaks at 232.9, 229.8, and 226.9 eV. The $3d_{5/2}$ peak with binding energy at 229.8 eV has a doublet $3d_{3/2}$ peak located at 232.9 eV, which corresponds to the molybdenite species (MoS_2) [41,42]. The 2*s* spectra located at 226.9 eV belongs to MoS_2 species [42]. The S 2*p* spectra depicted in Figure 13B match the binding energy of molybdenite at 162.6 eV and 163.8 eV for $2p_{3/2}$ and $2p_{1/2}$ [43,44], respectively. The Mo 3*d* spectra and S 2*p* spectra do not show any shifting in energy binding and there is no indication of oxide of molybdenum and sulfur species after H_2O_2 treatment on molybdenite surface. The effect of H_2O_2 on surface oxidation of molybdenite can be seen from O 1*s* spectra (Figure 13C). The peak located at 533.5 eV is assigned to the adsorption of oxygen on the molybdenite surface (O_2/MoS_2) [45]. The peak at 532.1 eV that corresponds to the oxide of the molybdenum species shifted to 532.0 eV after H_2O_2 treatment, supporting the low surface oxidation of molybdenite [11]. The oxidation products are observed in O 1*s* spectra rather than Mo 3*d* spectra, which may be due to the dissolution of molybdenum oxides during H_2O_2 treatment.

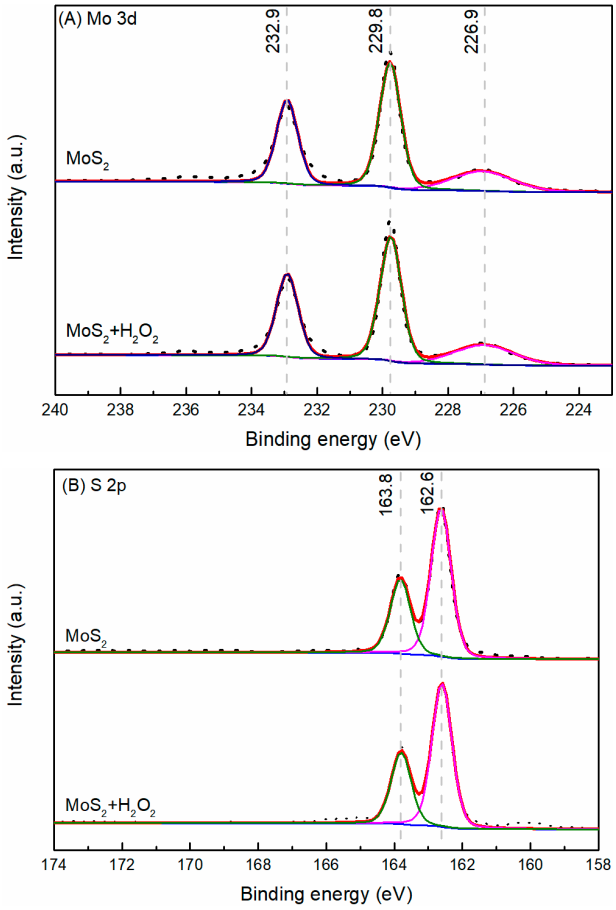

Figure 13. *Cont.*

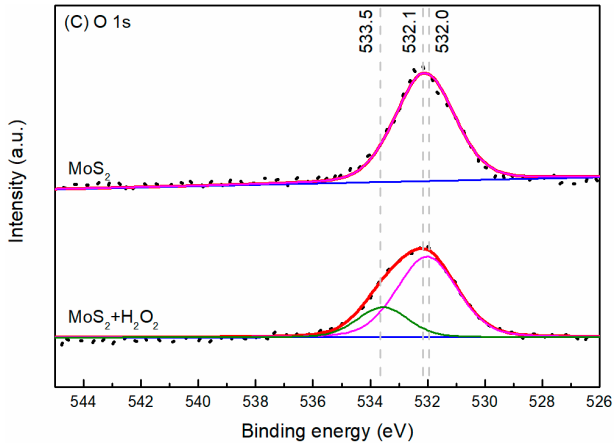

Figure 13. XPS spectra of molybdenite: (**A**) Mo 3*d*, (**B**) S 2*p*, (**C**) O 1*s*. Dots represent the experimental spectrum, heavy red solid lines indicate the best fit curve, and the individual XPS peaks are shown as thin solid lines in different colors.

In contrast with the molybdenite surface, there is significant difference in Bi 4*f*, S 2*s*, and O 1*s* of synthetic bismuthinite between untreated and treated surface. Figure 14A shows the XPS spectra of Bi 4*f*. Before H_2O_2 treatment, the highest intensity peaks are found at 158.3 and 163.6 eV, corresponding to the spin-orbit doublet of Bi $4f_{7/2}$ and Bi $4f_{5/2}$, respectively, of bismuth sulfide [46–48]. After H_2O_2 treatment, the presence of shoulders at higher energies of the doublet, 159.6 and 164.9 eV, are associated to the Bi–O bonds [49]. Figure 14B shows the S 2*s* spectra. The peak at 225.5 eV is in accordance with the Bi–S bond, which is characteristic of S 2*s* binding energy [50]. The new peak at 232.5 eV after H_2O_2 treatment is assigned to sulfate [51]. The O 1*s* spectra presented in Figure 14C are best fitted with two peaks located at 530.1 and 531.4 eV. The former peak corresponds to Bi–O species and the latter is attributed to surface hydroxyls respectively [52]. From the XPS analysis results, it can be easily concluded that H_2O_2 treatment had a negative effect on the bismuthinite surface due to the formation of oxidation products that precipitate on the bismuthinite surface and alter its surface hydrophobicity.

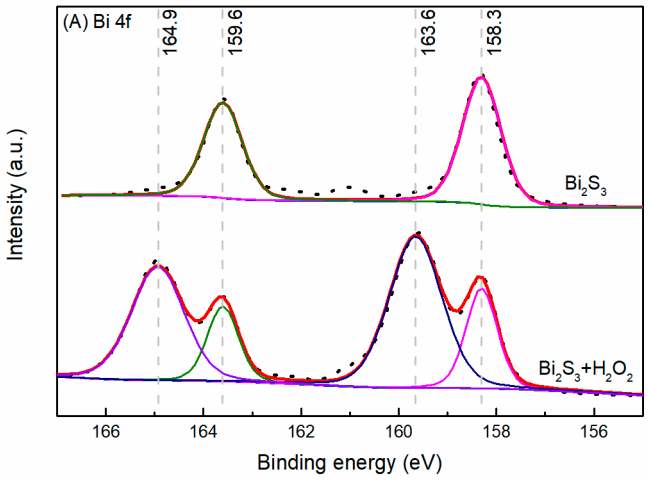

Figure 14. *Cont.*

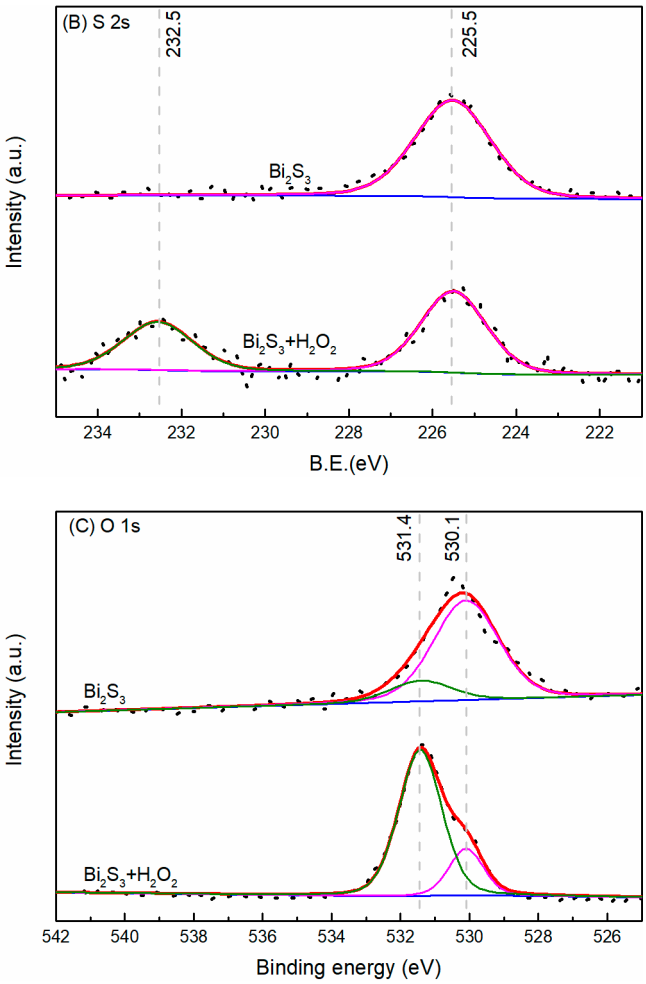

Figure 14. XPS spectra of bismuthinite: (**A**) Bi 4*f*, (**B**) S 2*s*, (**C**) O 1*s*. Dots represent the experimental spectrum, heavy red solid lines indicate the best fit curve, and the individual XPS peaks are shown as thin solid lines in different colors.

4. Conclusions

This study seeks to investigate the influence of H_2O_2 on the flotation performance of valuable minerals from Shizhuyuan ore. The following main observations and conclusions can be drawn:

(1) Increasing H_2O_2 concentration results in a decrease in the amount of solids and water recovery from the concentrate at pH 8, which indicates that the presence of H_2O_2 leads to gangue depression and lower froth stability.

(2) The recovery and grade of bismuthinite was drastically decreased from 50.14% and 1.71% to 4.64% and 0.22%, respectively, after adding H_2O_2, while that of molybdenite were slightly affected. This result suggests that the inhibition effect of H_2O_2 on flotation is much more pronounced for bismuthinite than in molybdenite.

(3) The flotation rate of bismuthinite was significantly lower than that of molybdenite, which demonstrates that bismuthinite floats more slowly than molybdenite. The addition of H_2O_2 marginally decreased the flotation rate of bismuthinite and showed a negligible influence on molybdenite.

(4) The results support the possibility of the selective separation of molybdenite and bismuthinite by applying H_2O_2 into flotation. The separation mechanism might probably be due to the precipitation of oxidation products (e.g., BiO) on the bismuthinite surface that enhances its

hydrophilicity. The oxidation products produced by H_2O_2 on the molybdenite surface dissolved into the solution (e.g., MoO_4^{2-}), maintaining its hydrophobicity.

Author Contributions: Y.H. and W.S. conceived and designed the experiments; S.L. performed the experiment; R.L. and S.L. analyzed the data and wrote the paper; H.H. contributed reagents/materials/analysis tools; and R.L. and S.L. wrote the paper.

Acknowledgments: This study was financially supported by the Fundamental Research Funds for the Central Universities of Central South University (No. 2018zzts223), National Natural Science Foundation of China (No. 51104179), the Collaborative Innovation Center for Clean and Efficient Utilization of Strategic Metal Mineral Resources, the National 111 Project (No. B14034), and the Key Laboratory of Hunan Province for Clean and Efficient Utilization of Strategic Calcium-containing Mineral Resources (No. 2018TP1002).

Conflicts of Interest: The authors declare no conflict of interest.

References

1. Chen, Y.; Li, H.; Sun, W.; Ireland, T.; Tian, X.; Hu, Y.; Yang, W.; Chen, C.; Xu, D. Generation of late mesozoic qianlishan a 2-type granite in nanling range, south China: Implications for shizhuyuan W-Sn mineralization and tectonic evolution. *Lithos* **2016**, *266*, 435–452. [CrossRef]
2. Yin, J.; Kim, S.J.; Lee, H.K.; Itay, T. K–Ar ages of plutonism and mineralization at the shizhuyuan W-Sn-Bi-Mo deposit, Hunan province, China. *J. Asian Earth Sci.* **2002**, *20*, 151–155. [CrossRef]
3. Cheng, Y.S. Petrogenesis of skarn in shizhuyuan W-polymetallic deposit, southern Hunan, China: Constraints from petrology, mineralogy and geochemistry. *Trans. Nonferr. Met. Soc. China* **2016**, *26*, 1676–1687. [CrossRef]
4. Zhao, P.; Yuan, S.; Mao, J.; Yuan, Y.; Zhao, H.; Zhang, D.; Shuang, Y. Constraints on the timing and genetic link of the large-scale accumulation of proximal W-Sn-Mo-Bi and distal Pb-Zn-Ag mineralization of the world-class dongpo orefield, Nanling range, south China. *Ore Geol. Rev.* **2018**, *95*, 1140–1160. [CrossRef]
5. Ding, F.; Zhan, J.; Wang, Z.; Chai, L.; Zhang, C. Simultaneous leaching of low grade bismuthinite and pyrolusite ores in hydrochloric acid medium. *Hydrometallurgy* **2016**, *166*, 279–284. [CrossRef]
6. Zhang, F.; Lin, R.; Zeng, Q.; Zhang, X. Experimental research on the beneficiation of Mo-Bi-W polymetallic ore from Jiangxi. *Metal. Mine* **2009**, *1*, 024.
7. Li, A. New process of flotation separation of associated Mo-Cu-Bi sulfide ore of xingluokeng tungsten ore. *Metal. Mine* **2012**, *4*, 74–78.
8. Han, Z.; Guan, Z. Status quo of research on copper-bismuth separation. *Metal. Mine* **2008**, *4*, 75–76.
9. Huang, P.; Cao, M.; Liu, Q. Using chitosan as a selective depressant in the differential flotation of Cu-Pb sulfides. *Int. J. Miner. Process.* **2012**, *106*, 8–15. [CrossRef]
10. Huang, P.; Wang, L.; Liu, Q. Depressant function of high molecular weight polyacrylamide in the xanthate flotation of chalcopyrite and galena. *Int. J. Miner. Process.* **2014**, *128*, 6–15. [CrossRef]
11. Suyantara, G.P.W.; Hirajima, T.; Miki, H.; Sasaki, K.; Yamane, M.; Takida, E.; Kuroiwa, S.; Imaizumi, Y. Selective flotation of chalcopyrite and molybdenite using H_2O_2 oxidation method with the addition of ferrous sulfate. *Miner. Eng.* **2018**, *122*, 312–326. [CrossRef]
12. Castro, S.; Lopez-Valdivieso, A.; Laskowski, J.S. Review of the flotation of molybdenite. Part I: Surface properties and floatability. *Int. J. Miner. Process.* **2016**, *148*, 48–58. [CrossRef]
13. Yuan, K. Study on cyanide free separation of Cu-Bi mixed concentrate. *Hunan Nonferr. Met.* **1988**, *1988*, 24–26.
14. Liu, Q.; Zhang, Y.; Laskowski, J.S. The adsorption of polysaccharides onto mineral surfaces: An acid/base interaction. *Int. J. Miner. Process.* **2000**, *60*, 229–245. [CrossRef]
15. Bulatovic, S.M. Use of organic polymers in the flotation of polymetallic ores: A review. *Miner. Eng.* **1999**, *12*, 341–354. [CrossRef]
16. Mu, Y.; Peng, Y.; Lauten, R.A. The depression of pyrite in selective flotation by different reagent systems—A literature review. *Miner. Eng.* **2016**, *96*, 143–156. [CrossRef]
17. Chimonyo, W.; Wiese, J.; Corin, K.; O'Connor, C. The use of oxidising agents for control of electrochemical potential in flotation. *Miner. Eng.* **2017**, *109*, 135–143. [CrossRef]
18. Nooshabadi, A.J.; Rao, K.H. Formation of hydrogen peroxide by galena and its influence on flotation. *Adv. Powder Technol.* **2014**, *25*, 832–839. [CrossRef]

19. Hirajima, T.; Miki, H.; Suyantara, G.P.; Matsuoka, H.; Elmahdy, A.M.; Sasaki, K.; Imaizumi, Y.; Kuroiwa, S. Selective flotation of chalcopyrite and molybdenite with H_2O_2 oxidation. *Miner. Eng.* **2017**, *100*, 83–92. [CrossRef]
20. Wang, D. *Development of Flotation Theory*; Science Press: Beijing, China, 1992; pp. 79–143.
21. Hu, Y.; Sun, W.; Wang, D. *Electrochemistry of Flotation of Sulphide Minerals*; Springer: Berlin, Germany, 2009; pp. 142–166.
22. Tao, D.; Luttrell, G.H.; Yoon, R.H. A parametric study of froth stability and its effect on column flotation of fine particles. *Int. J. Miner. Process.* **2000**, *59*, 25–43. [CrossRef]
23. Cho, Y.S.; Laskowski, J.S. Effect of flotation frothers on bubble size and foam stability. *Int. J. Miner. Process.* **2002**, *64*, 69–80. [CrossRef]
24. Ekmekçi, Z.; Bradshaw, D.J.; Allison, S.A.; Harris, P.J. Effects of frother type and froth height on the flotation behaviour of chromite in UG2 ore. *Miner. Eng.* **2003**, *16*, 941–949. [CrossRef]
25. Zheng, X.; Johnson, N.W.; Franzidis, J.P. Modelling of entrainment in industrial flotation cells: Water recovery and degree of entrainment. *Miner. Eng.* **2006**, *19*, 1191–1203. [CrossRef]
26. Chimonyo, W.; Corin, K.C.; Wiese, J.G.; O'Connor, C.T. Redox potential control during flotation of a sulphide mineral ore. *Miner. Eng.* **2017**, *110*, 57–64. [CrossRef]
27. Wiese, J.G. Investigating Depressant Behaviour in the Flotation of Selected Merensky Ores. Master's Thesis, University of Cape Town, Cape Town, South Africa, 2009.
28. Corin, K.C.; Wiese, J.G. Investigating froth stability: A comparative study of ionic strength and frother dosage. *Miner. Eng.* **2014**, *66*, 130–134. [CrossRef]
29. Wiese, J.G.; Harris, P.J.; Bradshaw, D.J. The effect of increased frother dosage on froth stability at high depressant dosages. *Miner. Eng.* **2010**, *23*, 1010–1017. [CrossRef]
30. Manono, M.S.; Corin, K.C.; Wiese, J.G. The effect of ionic strength of plant water on foam stability: A 2-phase flotation study. *Miner. Eng.* **2013**, *40*, 42–47. [CrossRef]
31. Xu, M. Modified flotation rate constant and selectivity index. *Miner. Eng.* **1998**, *11*, 271–278. [CrossRef]
32. Dowling, E.C.; Klimpel, R.R.; Aplan, F.F. Model discrimination in the flotation of a porphyry copper ore. *Miner. Metall. Process.* **1985**, *2*, 87–101.
33. Polat, M.; Chander, S. First-order flotation kinetics models and methods for estimation of the true distribution of flotation rate constants. *Int. J. Miner. Process.* **2000**, *58*, 145–166. [CrossRef]
34. Lynch, A.J.; Johnson, N.W.; Manlapig, E.V.; Thorne, C.G. *Mineral and Coal Flotation Circuits*; Elsevier Scientific Pub. Co.: Amsterdam, The Netherlands, 1981.
35. Wills, B.A.; Napiermunn, T.J. *Wills' Mineral Processing Technology: An Introduction to the Practical Aspects of Ore Treatment and Mineral Recovery*; Pergamon Press: Oxford, UK, 2006; pp. 651–659.
36. Agar, G.E. The optimization of flotation circuit design from laboratory rate data. In Proceedings of the 15th International Mineral Processing Congress, Cannes, France, 1985; p. 100.
37. Sheni, N.; Corin, K.; Wiese, J. Considering the effect of pulp chemistry during flotation on froth stability. *Miner. Eng.* **2018**, *116*, 15–23. [CrossRef]
38. Savassi, O.N. Direct Estimation of the Degree of Entrainment and the Froth Recovery of Attached Particles in Industrial Flotation Cells. Ph.D. Thesis, The University of Queensland, Queensland, Australia, 1998.
39. Kampf, A.R. HANDBOOK OF MINERALOGY, VOLUME: V. Borates, Carbonates, Sulfates. By John W. Anthony, Richard A. Bideaux, Kenneth W. Bladh, and Monte C. Nichols. Mineral Data Publishing, Tucson, Arizona; 2003, 813 p., $130 ($97.50 for MSA members). *Am. Mineral.* **2003**, *88*, 1842.
40. Mindat Org. Kornerupina: Mineral Data Publishing. Available online: https://www.mindat.org/min-2254.html (accessed on 5 September 2018).
41. Lince, J.R.; Carre, D.J.; Fleischauer, P.D. Effects of argon-ion bombardment on the basal plane surface of molybdenum disulfide. *Langmuir* **1986**, *2*, 805–808. [CrossRef]
42. Turner, N.H.; Single, A.M. Determination of peak positions and areas from wide-scan XPS spectra. *Surf. Interface Anal.* **1990**, *15*, 215–222. [CrossRef]
43. Benoist, L.; Gonbeau, D.; Pfister-Guillouzo, G.; Schmidt, E.; Meunier, G.; Levasseur, A. XPS analysis of lithium intercalation in thin films of molybdenum oxysulphides. *Surf. Interface Anal.* **1994**, *22*, 206–210. [CrossRef]
44. Stevens, G.C.; Edmonds, T. Electron spectroscopy for chemical analysis spectra of molybdenum sulfides. *J. Catal.* **1975**, *37*, 544–547. [CrossRef]

45. Zhuang, S.; Hall, W.K.; Ertl, G.; Knözinger, H. X-ray photoemission study of oxygen and nitric oxide adsorption on MoS_2. *J. Catal.* **1986**, *100*, 167–175.
46. Han, M.; Jia, J. The interlace of Bi_2S_3 nanowires with TiO_2 nanorods: An effective strategy for high photoelectrochemical performance. *J. Colloid Interface Sci.* **2016**, *481*, 91–99. [CrossRef] [PubMed]
47. Wang, Y.; Chen, J.; Jiang, L.; Sun, K.; Liu, F.; Lai, Y. Photoelectrochemical properties of Bi_2S_3 thin films deposited by successive ionic layer adsorption and reaction (SILAR) method. *J. Alloys Compd.* **2016**, *686*, 684–692. [CrossRef]
48. Xu, W.; Fang, J.; Chen, Y.; Lu, S.; Zhou, G.; Zhu, X.; Fang, Z. Novel heterostructured Bi_2S_3/Bi_2Sn2O_7 with highly visible light photocatalytic activity for the removal of rhodamine B. *Mater. Chem. Phys.* **2015**, *154*, 30–37. [CrossRef]
49. Díaz-Cruz, E.B.; Castelo-González, O.A.; Martínez-Alonso, C.; Montiel-González, Z.; Arenas-Arrocena, M.C.; Hu, H. Morphology control in microwave synthesized bismuth sulfide by using different bismuth salts. *Mater. Sci. Semicond. Process.* **2018**, *75*, 311–318. [CrossRef]
50. Kumar, D.R.; Kesavan, S.; Baynosa, M.L.; Nguyen, V.Q.; Shim, J.J. Flower-like Bi_2S_3 nanostructures grown on nitrogen-doped reduced graphene oxide for electrochemical determination of hydrogen peroxide. *J. Colloid Interface Sci.* **2018**, *530*, 361–371. [CrossRef] [PubMed]
51. Tamašauskaitė-Tamašiūnaitė, L.; Valiulienė, G.; Žielienė, A.; Šimkūnaitė-Stanynienė, B.; Naruškevičius, L.; Sudavičius, A. EQCM study on the oxidation/reduction of bismuth sulfide thin films. *J. Electroanal. Chem.* **2010**, *642*, 22–29. [CrossRef]
52. Mi, Y.; Li, H.; Zhang, Y.; Zhang, R.; Hou, W. One-pot synthesis of belt-like Bi_2S_3/BiOCl hierarchical composites with enhanced visible light photocatalytic activity. *Appl. Surf. Sci.* **2017**, *423*, 1062–1071. [CrossRef]